

# Genome Methylation Predicts Age and Longevity of Bats

Gerald S. Wilkinson<sup>1\*†</sup>, Danielle M. Adams<sup>1</sup>, Amin Haghani<sup>2</sup>, Ake T. Lu<sup>2</sup>, Joseph Zoller<sup>3</sup>, Charles E. Breeze<sup>4</sup>, Bryan D. Arnold<sup>5</sup>, Hope C. Ball<sup>6</sup>, Gerald Carter<sup>7</sup>, Lisa Noelle Cooper<sup>6</sup>, Dina K.N. Dechmann<sup>8,9,10</sup>, Paolo Devanna<sup>11</sup>, Nicolas J. Fasel<sup>12</sup>, Alexander V. Galazyuk<sup>6</sup>, Linus Günther<sup>13</sup>, Edward Hurme<sup>1,9</sup>, Gareth Jones<sup>14</sup>, Mirjam Knörnschild<sup>10,13</sup>, Ella Z. Lattenkamp<sup>11,15</sup>, Caesar Z. Li<sup>3</sup>, Frieder Mayer<sup>13</sup>, Josephine A. Reinhardt<sup>16</sup>, Rodrigo A. Medellín<sup>17</sup>, Martina Nagy<sup>13</sup>, Brian Pope<sup>18</sup>, Megan L. Power<sup>19</sup>, Roger D. Ransome<sup>14</sup>, Emma C. Teeling<sup>19</sup>, Sonja C. Vernes<sup>11,20,21</sup>, Daniel Zamora-Mejías<sup>17</sup>, Joshua Zhang<sup>2</sup>, and Steve Horvath<sup>2,3\*†</sup>

*1 Department of Biology, University of Maryland, College Park 20742 USA*

*2 Department of Human Genetics, David Geffen School of Medicine, University of California, Los Angeles 90095 USA*

*3 Department of Biostatistics, Fielding School of Public Health, University of California, Los Angeles 90095 USA*

*4 AltiUS Institute for Biomedical Sciences, Seattle, WA, 98121 USA*

*5 Department of Biology, Illinois College, Jacksonville, IL 62650 USA*

*6 Department of Anatomy and Neurobiology, Northeast Ohio Medical University, Rootstown, Ohio, U.S.A. 44272-0095*

*7 Department of Evolution, Ecology and Organismal Biology, The Ohio State University, 318 W. 12th Avenue, Columbus, OH, 43210 USA*

*8 Department of Migration, Max Planck Institute of Animal Behavior, Radolfzell, Germany*

*9 Department of Biology, University of Konstanz, Konstanz, Germany*

*10 Smithsonian Tropical Research Institute, Panama*

*11 Neurogenetics of Vocal Communication Group, Max Planck Institute for Psycholinguistics, Nijmegen, The Netherlands*

*12 Department of Ecology and Evolution, University of Lausanne, Lausanne, Switzerland*

*13 Museum für Naturkunde, Leibniz-Institute for Evolution and Biodiversity Science, Berlin, Germany*

*14 School of Biological Sciences, University of Bristol, Bristol, UK*

*15 Department Biology II, Ludwig Maximilians University Munich, Martinsried, Germany*

*16 Department of Biology, State University of New York, Geneseo 14454 USA*

*17 Instituto de Ecología, Universidad Nacional Autónoma de México, Ap. Postal 70-275 04510, Ciudad Universitaria, México*

*18 Lube Bat Conservancy, 1309 NW 192nd Avenue, Gainesville, FL 32609 US*

*19 School of Biology and Environmental Science, University College Dublin, Belfield, Dublin 4, Ireland*

*20 Donders Institute for Brain, Cognition and Behaviour, Nijmegen, The Netherlands*

*21 School of Biology, The University of St Andrews, Fife, UK*

\*Corresponding authors: [wilkinso@umd.edu](mailto:wilkinso@umd.edu) and [shorvath@mednet.ucla](mailto:shorvath@mednet.ucla)

†These authors jointly supervised this work: G.S. Wilkinson, S. Horvath

## **Abstract**

Exceptionally long-lived species, including many bats, rarely show overt signs of aging, making it difficult to determine why species differ in lifespan. Here, we use DNA methylation (DNAm) profiles from 712 known-age bats, representing 26 species, to identify epigenetic changes associated with age and longevity. We demonstrate that DNAm accurately predicts chronological age. Across species, longevity is negatively associated with the rate of DNAm change at age-associated sites. Furthermore, analysis of several bat genomes reveals that hypermethylated age- and longevity-associated sites are disproportionately located in promoter regions of key transcription factors (TF) and enriched for histone and chromatin features associated with transcriptional regulation. Predicted TF binding site motifs and enrichment analyses indicate that age-related methylation change is influenced by developmental processes, while longevity-related DNAm change is associated with innate immunity or tumorigenesis genes, suggesting that bat longevity results from augmented immune response and cancer suppression.

## **Introduction**

DNA methylation (DNAm) influences many processes including development<sup>1</sup>, gene regulation<sup>2</sup>, genomic imprinting<sup>3</sup>, X chromosome inactivation<sup>4</sup>, transposable element defense<sup>5</sup>, and cancer<sup>6</sup>. Over 75% of cytosine-phosphate-guanine (i.e. CpG) sites are typically methylated in mammalian cells, but global DNAm declines with age, which can lead to loss of transcriptional control and either cause, or contribute to, deleterious aging effects<sup>7</sup>. Conversely, DNAm often increases (i.e., shows hypermethylation) at CpG islands, which are

CpG-dense regions often found in gene promoter regions near transcription start sites (tss)<sup>8,9,10</sup>. Age-related changes in DNAm can be used to predict biological age in humans<sup>11,12</sup> and are beginning to be used to predict age in other species<sup>13,14,15,16,17</sup>. Given that aging of wild animals typically requires long-term mark-recapture data or lethal tissue sampling, an accurate, noninvasive aging method would enable study of age-associated changes in traits critical for survival, such as sensory perception, metabolic regulation, and immunity in a variety of long-lived species.

DNAm has also been used to predict lifespan in humans<sup>18,19,20</sup>. Intriguingly, interventions known to increase lifespan in mammals, such as caloric restriction, reduce the rate at which methylation changes<sup>21,22</sup>. Moreover, comparison of age-related changes in DNAm across species<sup>22,23</sup> suggests that DNAm rate also varies with lifespan. However, interspecific studies have so far used different methods on a few primate, rodent, or canid species<sup>22,23</sup> making it difficult to determine reasons for methylation differences.

The distribution and function of genomic regions that exhibit age or longevity-related changes in DNAm are not fully understood<sup>20,24</sup>. In humans, hypermethylated age-associated CpG sites tend to be near genes predicted to be regulated by transcription factors involved in growth and development, whereas hypomethylated sites are near genes from more disparate pathways<sup>25</sup>. A recent study in dogs also found that age-related hypermethylated sites are near genes that influence developmental processes<sup>17</sup>. Human aging has been associated with modification of histone marks and relocalization of chromatin modifying factors in a tissue-dependent manner<sup>26</sup>. Comparative analysis of CpG density in conserved gene promoter regions has revealed that CpG density is positively related to lifespan in mammals<sup>27</sup>, as well

as other vertebrates<sup>28</sup>, but the genes involved were not enriched for any pathway or biological process.

Bats have great potential for providing insight into mechanisms that reduce deleterious aging effects because species from multiple independent lineages have maximum lifespans more than four times greater than similar-sized mammals<sup>29</sup> despite tolerating high viral loads<sup>30,31</sup> and showing few signs of aging. Here, we use a custom microarray that assays 37,492 conserved CpG sites to measure DNAm from known-aged individuals of 26 species of bats and address three questions. 1) How accurately can chronological age be estimated from DNAm for a long-lived species within a mammalian order? 2) Does age-related change in DNAm predict maximum lifespan? 3) What genes are nearest the sites where DNAm changes as a function of age or differences in longevity between species? We find that DNAm can predict age of individuals with high accuracy. At the species level, the rate of change in DNAm at age-associated sites also predicts maximum lifespan. CpG sites that are informative for age or longevity are more likely to gain methylation and be near promoter regions of transcription factors involved in developmental processes. Longevity-associated sites are, in addition, enriched for genes involved in cancer suppression or immunity.

## Results

**Predicting individual age using DNA methylation.** DNAm profiles were analyzed from 712 wing tissue biopsies taken either from captive or free-ranging individuals of known age representing 26 species and six families of bats. Probe sequences were mapped in the genomes of nine of these species (Supplementary Table 1) and a total of 35,148 probes were located in at least one bat genome. For the 2340 probes not mapped in any bat, the median

DNAm mean (0.496) and coefficient of variation (CV = 0.051%), were nearly identical to the 62 human SNP probes on each array (median mean = 0.500, median CV = 0.032%). In contrast, probes that mapped to at least one bat had DNAm means ranging from 0.006 to 0.995 with a median of 0.634. To predict age, we used sites mapped in one or more species from the taxonomic group of interest, i.e. order, genera or species.

Similar to human epigenetic clocks<sup>12,20</sup>, elastic-net regression accurately predicted chronological age from a linear combination of DNAm beta values (henceforth DNAmAge) using 162 CpG sites. Leave-one-out (LOO) cross-validation shows that DNAm can predict age with a median absolute error (MAE) of 0.74 years (Fig. 1a). Limiting the analysis to smaller taxonomic groups (species or genera) can improve accuracy if sufficient data are available. For example, the correlation between chronological and DNAmAge in a LOO cross-validation analysis for 40-50 samples from a single species can be 0.96 or higher (Fig. 1b,c; Supplementary Fig. 1); a similar analysis on 176 samples from six *Pteropus* species gave a correlation of 0.97 (MAE = 0.77, Supplementary Fig. 2b). Thus, DNAm from a wing tissue sample for any of these species can reveal the animal's age at the time of sampling to within a year.

To assess how well DNAm might predict age in a species not represented by our samples, we conducted a second cross-validation analysis in which data for one species was left out (leave-one-species out; LOSO) and ages were predicted for that species using a clock estimated from the remaining 25 species. This analysis (Fig. 1d) resulted in a correlation between observed and predicted age of 0.84 (MAE = 1.41 years). The LOSO analysis also showed that DNAm consistently underestimates age in some species, while overestimating age in others. For example, *Desmodus rotundus* (sp. 5, Fig. 1d) samples exhibit lower values

of DNAmAge (suggesting lower aging rates) than *Phyllostomus hastatus* (sp. 15, Fig. 1d) samples, consistent with the longer lifespan of *D. rotundus*<sup>29</sup>.

**Predicting species longevity from DNA methylation.** To determine if the rate of DNAm change predicts variation in maximum lifespan among species, we incorporated a recent bat phylogeny<sup>32</sup> into a generalized least squares regression (PGLS) to predict the longevity quotient (LQ) - the ratio of observed to expected maximum lifespan for a mammal of the same body size<sup>29</sup>. We first identified a common set of age-associated CpG sites for this analysis by conducting a meta-analysis of all age-DNAm correlations by probe for 19 bat species with 15 or more samples (Methods). The top 2000 age-associated sites (henceforth, age differentially methylated positions or age DMPs) consist of 1165 sites that show age-associated hypermethylation and 835 sites exhibiting age-associated hypomethylation. Both mean rates of hypermethylation and hypomethylation predict LQ, such that long-lived species have lower rates of DNAm change (Fig. 2a,b). A PGLS analysis on maximum lifespan with body mass as a covariate gave very similar results (Supplementary Table 2). Assuming that the rate of change in DNAm reflects epigenetic stability, these results suggest that better epigenetic maintenance is associated with longer maximum lifespan, independent of body size, across bats.

**Identifying age and longevity-associated genes.** To identify DMPs associated with differences in LQ (henceforth longevity DMPs), we compared relationships between DNAm and age for three long-lived species and two short-lived species (cf. Fig. 2) from four bat families. Longevity DMPs have a significant (BY FDR = 0.05) interaction term between age

and longevity type in a linear mixed model with species as a random effect (see Methods, Supplementary Fig. 3). We identified 1491 longevity DMPs, including 694 in which short-lived species gain DNAm faster with age and 797 in which short-lived species lose DNAm faster.

Age and longevity DMPs are widely distributed in the genome, but differ in relative abundance across chromosomes (Fig. 3a,b). For example, of the 1077 probes that map to chromosome 1 (syntenic with the human X chromosome) in *R. ferrumequinum* (a long-lived bat with the most mapped probes, 30,724, Supplementary Table 1) only 12 are age-associated while 46 are longevity-associated. Not surprisingly, 596 of 753 sites (79.2%) that differ in DNAm values between the sexes across species are on the *R. ferrumequinum* X chromosome. Sex DMPs are independent of age DMPs (6.1% overlap,  $P = 0.32$ , Fisher's Exact Test, FET) and longevity DMPs (5.2% overlap,  $P = 0.10$ , FET). When limited to promoter regions, almost all age and longevity DMPs exhibit hypermethylation (Fig. 3c). Change in DNAm with respect to age correlates with change in DNAm with respect to longevity ( $r = 0.454$ ,  $P < 0.0001$ ), which results in significant overlap among longevity and age DMPs ( $P < 0.0001$ , FET, Fig. 3d and Supplementary Fig. 5a) and among unique genes near those DMPs (Fig. 3e and Supplementary Fig. 5b).

Even though about 7,000 unique CpG probe sequences on the mammalian methylation array are unmapped in a bat genome (Supplementary Table 2), the mapped CpG sites are typically (median = 93%) nearest the same gene in any pair of bats (Supplementary Fig. 4c). Furthermore, genomic regions occupied by age and longevity DMPs are similar among bat species (Supplementary Fig. 4). For example, 68% of 2874 probes that map to a promoter region in the short lifespan species, *M. molossus*, also map to a promoter region in the

distantly related long lifespan species, *R. ferrumequinum* (Fig. 4b). Promoter regions are enriched for hypermethylating, but not hypomethylating, age and longevity DMPs in *M. molossus* (Fig. 4c,d) and other bats (Supplementary Fig. 5c,d). In bat genomes where CpG islands have been identified (e.g. *R. ferrumequinum*) hypermethylating age DMPs are much more likely than hypomethylating age DMPs to be located in CpG islands ( $P < 0.0001$ , FET); the same is true for longevity DMPs ( $P < 0.0001$ , FET).

Given that regions near promoters contain more age and longevity DMPs than expected, we evaluated the genes nearest those DMPs for possible functions. In view of the overlap in age and longevity DMPs, not surprisingly, genes with age or longevity DMPs in promoter regions show similar patterns of enrichment among biological process categories, i.e. developmental process, transcription, and regulation of transcription are enriched in *M. molossus* (Fig. 4e). Genes with age DMPs in promoter regions are further enriched for multicellular organism development. With regard to protein class, gene lists for both age and longevity DMPs are enriched for homeodomain transcription factors containing helix-turn-helix motifs (Fig. 4f). These patterns are characteristic of other bat species, too (Supplementary Fig. 6), although the gene list composition varies. For example, 142 hypermethylated age genes were identified across the four bat genomes used for identifying longevity DMPs. Of these genes, 89 exhibited the same DMP-gene association in at least 3 of the 4 genomes.

Comparisons between the age and longevity-related genes and several relevant gene lists provide additional evidence for gene function. For example, hypermethylated age genes in bats strongly overlap hypermethylated age genes recently reported for dogs<sup>17</sup> (e.g. 83 of 143 hypermethylated dog genes are also related to age in the short lifespan *M. molossus*,  $P =$



4.57e-54, FET). In contrast, only 5 of 60 hypomethylated dog genes are related to age in *M. molossus* ( $P = 0.21$ , FET). *Molossus molossus* age genes are not enriched for immunity genes ( $P = 0.241$ , FET) or genes that frequently mutate in cancer ( $P = 0.205$ , FET). However, *M. molossus* longevity genes exhibit significant overlap with genes involved in immunity ( $P = 0.002$ , FET) and genes frequently mutated in human tumors ( $P = 0.016$ , FET, Fig. 4g). Similar overlap patterns among immunity, longevity and tumor-mutated genes also exist for long-lived bats (Supplementary Fig. 6).

While methylation in a promoter region can influence transcription, transcription regulation can also result from interactions among DNA-bound proteins that are in proximity due to chromatin folding<sup>33</sup>. To evaluate the possibility of either short or long-range transcriptional regulation, we used eFORGEv.2.0<sup>34</sup> to predict how DMPs likely influence regulatory regions. This program first identifies probe sequences as being associated with five core histone marks or 15 predicted chromatin states in prior epigenomic studies using over 100 cell lines from multiple tissue sources, then uses permutation tests against the species genomic background to determine which histone marks or chromatin states occur nonrandomly. Using probes mapped in the long lifespan species *Desmodus rotundus* as background, we find that age and longevity DMPs exhibiting hypermethylation are enriched for repressive histone H3 trimethylated at lysine27 (H3K27me3) and active H3K4me1 marks in relevant cell lines (Fig. 5a, b). Hypomethylated age DMPs are enriched in all tissues for H3K9me3, while hypomethylated longevity DMPs show no enrichment (Fig. 5a, b). Analysis of predicted chromatin states reveals that hypermethylated age DMPs are enriched in all tissues for repressed polycomb complexes, while hypomethylated age DMPs are enriched for quiescent chromatin states (Fig. 5c). Longevity DMPs, both hypermethylating and

hypomethylating, also show enrichment for quiescent states, as well as enrichment for repressive polycomb complexes or enhanced bivalent states in some tissues (Fig. 5d).

Transcription factor (TF) motifs identified in DMP probe sequences that are involved in cell cycle regulation and genome stability are enriched among hypermethylating age sites (Fig. 5e). Several of those transcription factors, including cut-like homeobox 1 (CUX1), AT-rich interaction domain 3A (ARID3), and E2F transcription factor 1 (E2F) are involved in cell cycle regulation<sup>35,36,37</sup>, while others, such as zinc finger protein 161 (ZFP161), are involved in genome stability<sup>38</sup>. In contrast, hypomethylating age sites only overlap three TF clusters, one of which, IRF7, is a master regulator of the interferon-dependent innate immune response in bats<sup>39</sup>.

Longevity TF motifs are largely independent of age TF motifs (Fig. 5e), with one exception, c203-transcription factor AP-2 gamma (TFAP2C), which is involved in epidermal cell lineage commitment<sup>40</sup> and regulation of tumor progression<sup>41</sup>. The other longevity TF motifs also have known associations with tumorigenesis. GCM1/3 binds to pleiomorphic adenoma gene-like 1 (Plagl1), which codes for a protein that suppresses cell growth. This gene is often methylated and silenced in cancer cells<sup>42</sup>. CNOT3 acts as a tumor suppressor in T-cell acute lymphoblastic leukemia (T-ALL)<sup>43</sup> but can also facilitate development of non-small cell lung cancer<sup>44</sup>. Finally, HIC1, hypermethylated in cancer 1 protein, acts as a tumor suppressor and is involved in regulation of p53 DNA damage responses<sup>45</sup>. Only a single TF motif, HD/5 in the BARHL2 group<sup>46</sup>, was associated with hypomethylated longevity DMPs.

Enrichment analyses<sup>47</sup> using the age and longevity gene lists for *M. molossus* identify several key regulators that are significantly associated with hypermethylated sites, but none with hypomethylated sites (Fig. 5f and Supplementary Fig. 6c). Orthodenticle homeobox 2

(OTX2) and RE1 silencing transcription factor (REST) are associated with both age and longevity, whereas other predicted TFs largely differ between age and longevity. REST is induced during human aging and represses neuronal genes that promote cell death<sup>48</sup>. Note that four of nine transcription regulators predicted to be associated with longevity frequently undergo mutations in human tumors and three are involved in innate immunity (Fig. 5f).

## Discussion

As with other species<sup>13,14,17,49</sup>, age-related changes in DNAm occur throughout bat genomes. While 162 CpG sites are sufficient to predict chronological age, these represent only a small fraction of the sites that correlate with age, because penalized regression excludes highly correlated variables to avoid multi-collinearity. Consequently, we carried out a meta analysis that correlated methylation at individual CpG sites with age across species to identify age DMPs. At these sites, long-lived species exhibit a lower rate of change in DNAm, while short-lived species exhibit faster increases in DNAm. How those changes contribute to longevity is not entirely clear, but our results suggest several key transcriptional regulators are involved and modulate the rate at which DNAm changes between short and long-lived species.

Our results are consistent with an epigenetic clock theory of aging that connects beneficial developmental and cell maintenance processes to detrimental processes causing tissue dysfunction<sup>20</sup>. A large body of evidence links age-related hypermethylated sites to genes and genomic regions that influence developmental processes<sup>9,10,17</sup>. We find that the sites that gain DNAm with age also tend to be in CpG islands, consistent with studies in humans<sup>50</sup>. But, in contrast, we find little enrichment for genes associated with hypomethylated sites, and

these genes are less likely to be shared across species. We interpret these results to indicate that DNAm loss with age is widespread and not concentrated in particular pathways. DNAm gain with age, on the other hand, occurs predictably near genes involved in many of the same developmental processes in humans, mice, dogs and bats, consistent with a shared mammalian origin.

Our analyses are based entirely upon wing biopsy samples and the reported DNAm patterns could differ by tissue, as has been frequently observed<sup>8</sup>. However, bat wing tissue is capable of unusually rapid regeneration<sup>51</sup> and consists of multiple tissue types<sup>52</sup>, making it particularly useful for measuring age-related changes in DNAm. Additionally, these non-lethal biopsies are relatively easy to obtain from wild-caught bats, thus allowing for future longitudinal and cross-sectional studies of epigenetic aging.

DNAm of genes suppressed in stem cells is a hallmark of cancer<sup>10</sup>. Several lines of evidence suggest that bat genes with longevity DMPs are important for cancer suppression and provide enhanced immunity. First, these genes disproportionately include many known to mutate frequently in human cancers or involved in innate immunity. Second, several transcription factors identified by motif analysis act as tumor suppressors, such that if they are silenced by methylation in older individuals, tumor formation should be more likely. Third, among the transcription factors identified from the list of genes with hypermethylated sites in promoter regions, several of them mutate in human cancers. While bats are not immune from cancer<sup>53</sup>, genetic adaptations for tumor suppression have been described for *Myotis brandtii*<sup>54</sup> and *M. myotis*<sup>55</sup> to help explain the extreme longevity of those species. Bats also have genetic mechanisms that enable strong antiviral immune responses without inducing damaging inflammatory reactions that may enable them to tolerate high levels of viral exposure<sup>30,31,56</sup>.

The results of this study are consistent with the hypothesis that enhanced epigenetic stability, especially associated with innate immunity and cancer suppression genes, facilitates the exceptional longevity in bats.

## Methods

**Wing tissue samples.** Wing punches were taken from 778 individually marked animals that were either kept in captivity (15 species) or recaptured as part of long-term field studies (11 species). We excluded 42 samples because we did not have independent evidence to confirm minimum age estimates. For 630 samples the individual was marked shortly after birth, so age estimates were exact. For the remainder, age represented a minimum estimate because the individual was not initially banded as a juvenile. We used minimum age estimates when other evidence, such as tooth wear or time since initial capture, indicated that the minimum age estimate was likely to be close to the real age. In the Supplementary Methods, we provide additional information on when and where samples were taken from either captive or free-ranging animals.

After extraction DNA concentration was estimated with a QuBit and samples were concentrated, if necessary, to reach a minimum of 10 ng/μl in 20 μl. To estimate rates of methylation we limit analyses to the 23 species for which we had more than 10 samples from known-aged individuals. Maximum lifespan for each species was obtained from<sup>29</sup> or from captivity records and is listed along with the range of ages of individuals sampled in Table 1.

**DNA methylation profiling.** All methylation data were generated using a custom Illumina methylation array (HorvathMammalMethylChip40) based on 37492 CpG sites<sup>57</sup>. Out of these

37492 sites, 1951 were selected based on their utility for human biomarker studies; these CpGs, which were previously implemented in human Illumina Infinium arrays, were selected due to their relevance for estimating human age. The remaining 35541 probes were chosen due to their location in highly conserved 50 bp sequences with a terminal CpG site. The particular subset of species for each probe is provided in the chip manifest file at the NCBI Gene Expression Omnibus (GEO) platform (GPL28271). Five bat genomes, *Pteropus vampyrus*, *P. alecto*, *Eptesicus fuscus*, *Myotis davidii* and *M. lucifugus*, were used in the design of the array.

Bisulfite conversion of DNA samples using the Zymo EZ DNA Methylation Kit (ZymoResearch, Orange, CA, USA), as well as subsequent hybridization and scanning (iScan, Illumina), were performed according to the manufacturers' protocols by applying standard settings. DNA methylation levels ( $\beta$  values) were determined by calculating the ratio of intensities between methylated (signal A) and unmethylated (signal B) sites. Specifically, the  $\beta$  value was calculated from the intensity of the methylated (M corresponding to signal A) and unmethylated (U corresponding to signal B) sites, as the ratio of fluorescent signals  $\beta = \text{Max}(M,0)/[\text{Max}(M,0) + \text{Max}(U,0) + 100]$ . Thus,  $\beta$  values range from 0 (completely unmethylated) to 1 (completely methylated). The SeSaMe method<sup>58</sup> was used to normalize  $\beta$  values for each probe. A cluster analysis by species identified 24 samples as outliers, likely due to their low DNA concentrations. After excluding these, along with the 42 excluded due to insufficient age information, we retained 712 of the 778 samples for further analysis.

**Probe mapping and annotation.** We used sequences and annotations for ten bat genomes (Supplementary Table 1), which include six recently published reference assemblies [19], to

locate each 50 bp probe on the array. The alignment was done using the QUASR package<sup>59</sup> with the assumption for bisulfite conversion treatment of the genomic DNA. For each species' genome sequence, QUASR creates an in-silico-bisulfite-treated version of the genome. The set of nucleotide sequences of the designed probes, which includes degenerate base positions due to the bisulfite conversion, was expanded into a larger set of nucleotide sequences representing every possible combination of degenerate bases. We then ran QUASR (a wrapper for Bowtie2) with parameters -k 2 --strata --best -v 3 and bisulfite = "undir" to align the enlarged set of probe sequences to each prepared genome. From these files, we collected only alignments where the entire length of the probe perfectly matched to the genome sequence (i.e. the CIGAR string 50M and flag XM=0).

Following the alignment, the CpGs were annotated based on the distance to the closest transcriptional start site using the ChIPseeker package<sup>60</sup>. A gff file with these was created using these positions, sorted by scaffold and position, and compared to the location of each probe in BAM format. We report probes whose variants only mapped to one unique locus in a particular genome. Gene annotations for the ten bat genomes are available at <http://hdl.handle.net/1903/26373>.

Genomic location of each CpG was categorized as intergenic, 3' UTR, 5' UTR, promoter region (minus 10 kb to plus 1000 bp from the nearest TSS), exon, or intron. We identified X-linked probes in bat genomes by comparison to probes mapped to the X for the human genome, HG19. Tests for enrichment among genomic categories were performed with contingency or Fisher's Exact tests (FET) in JMP Pro v14.1 for the four species used to identify longevity-associated sites, i.e. one short-lived bat, *Molossus molossus*, and three long-lived bats, *Myotis myotis*, *Desmodus rotundus* and *Rhinolophus ferrumequinum*,

representing four different bat families. We did not include *Leptonycteris yerbabuenae* in these analyses because no genome is available for that species. While most sites map to the same nearest gene, some differences exist. In the text, we present enrichment results for the short-lived species, *M. molossus*, but provide parallel results in Supplementary Figures for one or more of the long-lived species, *R. ferrumequinum*, *D. rotundus* and *M. myotis*.

**Creation of epigenetic clocks using penalized regression.** We developed epigenetic clocks for bat wing tissue by regressing chronological age on all CpGs that map to at least one of the ten bat genomes. To improve linear fit we transformed chronological age to  $\sqrt{\text{age}+1}$ . Penalized regression models were created in the R package “glmnet”<sup>61</sup>. We investigated models produced by “elastic net” regression ( $\alpha=0.5$ ). The optimal penalty parameters in all cases were determined automatically by using a 10-fold internal cross-validation (cv.glmnet) on the training set. By definition, the alpha value for the elastic net regression was set to 0.5 (midpoint between Ridge and Lasso-type regression) and was not optimized for model performance. We performed two cross-validation schemes for arriving at unbiased estimates of the accuracy of the different DNAm based age estimators. One type consisted of leaving out a single sample (LOO) from the regression, predicting an age for that sample by regressing an elastic net on the methylation profiles of all other samples, and iterating over all samples. We conducted LOO analyses using all samples from all species, using all samples from each species, and using all samples from several species in the same genus. The second type consisted of leaving out a single species (LOSO) from the regression, thereby predicting the age of each sample using the data for all other species.



**Identification of differentially methylated positions for age and longevity.** To identify differentially methylated positions (DMPs) associated with age, we computed the Pearson correlation coefficient between methylation level ( $\beta$ ) and chronological age for each of the 37,492 sites for the 19 species with 15 or more samples (Table 1). The significance of each site across species was then evaluated using Stouffer's unweighted z-test<sup>62</sup>. CpG sites were ranked by significance and the top 2000 sites based on the correlation with untransformed age were selected for subsequent analyses and are referred to as age DMPs. For probes with contrasting patterns in different species, methylation direction was assigned based on the most frequent direction across species to ensure mean methylation rates are comprised of the same set of sites in each species. Because we used all sites on the array, some sites do not map to a unique position in one or more bat genomes. Supplementary Table 1 indicates how many sites map to each species.

To identify DMPs associated with longevity we compared methylation rates between three long-lived species (*R. ferrumequinum*, *D. rotundus*, and *M. myotis*) and two short-lived species (*M. molossus* and *L. yerbabuenae*). We chose these five species because they represent three independent lineages of increased longevity<sup>29</sup> and because high-quality genome assemblies are available for four of them<sup>63</sup>. We used a linear mixed-effects model (nlme) to fit methylation level ( $\beta$ ) as a function of transformed chronological age ( $\sqrt{\text{age} + 1}$ ), longevity category, and their interaction, with species included as a random effect. We defined probes as longevity-associated if the p-value of the interaction term was less than 0.05 after Benjamini-Yekutieli (BY) false discovery rate (FDR) correction<sup>64</sup>. In this analysis, a positive interaction means a steeper positive slope for the short-lived species relative to the long-lived species. If the main effect of age is positive (hypermethylation) and the interaction

is positive, then short-lived species are gaining methylation faster. If the main effect is negative and the interaction is negative, then short-lived species are losing methylation faster.

**Phylogenetic analysis of bat longevity.** Using phylogenetic generalized least squares regression (PGLS) we tested the effect of mean rate of methylation change on longevity using both the longevity quotient (LQ) and maximum longevity (log-transformed). LQ is the ratio of the observed species maximum lifespan to the maximum lifespan predicted for a nonflying placental mammal of the same body mass<sup>29</sup>. We present results for LQ in the text and for a model containing both log(maximum longevity) and log(mass) in Supplementary Table 2. For each species with at least 10 known-age samples, we calculated the mean rates of hypermethylation and hypomethylation using the top 2000 age-associated DMPs as described above. Hypermethylation and hypomethylation rates were tested separately. Phylogenetic relationships among bats are based on a recent maximum likelihood tree<sup>32</sup>. Models were fit via maximum likelihood using the “glS” function of the “nlme” package in R v.3.1-143 and assume a Brownian model of trait evolution.

**Probe and gene enrichment analyses.** To determine how changes in methylation influence age and longevity, we conducted enrichment analyses on the CpG probes and on the genes nearest to them. We used eFORGE 2.0<sup>34</sup> to test for enrichment among age or longevity DMPs that either increase or decrease in methylation in comparison with five histone marks and 15 chromatin states mapped in cell lines by the Epigenomics Roadmap Consortium (<http://www.ncbi.nlm.nih.gov/epigenomics>). Bat wing tissue is unusual in that it contains epithelial skin, muscle, blood and elastin<sup>52</sup>. Consequently, we limited enrichment analyses to

data from cell lines derived either from skin, blood or muscle. We also restricted the analysis to probes mapped in a bat genome at least 1 kb apart. We used *Demodius rotundus* to provide a background probe set but obtained very similar results by using other bat genomes, e.g. *Eptesicus fuscus* or *Pteropus vampyrus*, available in eFORGE as backgrounds for the mammalian methylation array. We present enrichment values for each DMP set as the  $-\log_{10}$  p binomial value and consider those outside the 95th percentile of the binomial distribution after correction for multiple testing<sup>64</sup> as significant.

We identified putative transcription factors that could utilize open chromatin and bind to the DNA by testing for enrichment in each DMP set for predicted binding sites among the probes on the mammalian methylation array. Binding sites were included if their FIMO (Find Individual Motif Occurrence) p-value was less than  $10e-5$ . FIMO scans were performed using the MEME suite (v.4.12.0, available at <http://meme-suite.org/doc/download.html>). Bedtools (v.2.25.0) was used to intersect the mammalian methylation array file and provide probe-to-TF motif annotations. We then used a hypergeometric test (phyper) to evaluate overlap between probe sets and transcription factor motifs obtained from four transcription factor databases: TRANSFAC<sup>65</sup>, UniPROBE<sup>66</sup>, HT-Selex<sup>67</sup>, and JASPAR<sup>68</sup>. Redundant transcription factor motifs were then consolidated into clusterscf.<sup>69</sup> to identify distinct transcription factors. Function was inferred using information derived primarily from studies in mouse and humans<sup>46</sup>.

We used several approaches for determining the type and function of genes associated with age and longevity DMPs. First, we identified the gene (using human orthologs) with the nearest transcription start site to every mapped probe for each of the four species, *R. ferrumequinum*, *Desmodius rotundus*, *Myotis myotis* and *Molossus molossus*, used to identify

longevity DMPs. We then used the subsequent lists of unique genes for each species as background for enrichment tests. While the number of probes near the same gene varies considerably, on average, each unique gene is near five or six probes. Thus, the number of unique genes with an identifiable human ortholog near a probe was 4918 in *R.*

*ferrumequinum*, 4693 in *M. molossus*, 4611 in *M. myotis* and 4534 in *D. rotundus*, reflecting the variation in the number of mapped probes (Supplementary Table 1). Given that the probes were designed to align to regions conserved across all mammals, we suspect some of the differences among species in gene associations reflect variation in genome assembly or annotation. In addition, an important caveat to keep in mind is that the CpGs on the array do not randomly sample the genome<sup>57</sup>. Thus, even when we use mapped probes or the genes near them as background for enrichment tests, there is potential for bias given that the probes are in conserved regions. We assumed a gene was associated with hypermethylated DMPs if it had more hypermethylated than hypomethylated sites nearest its transcription start site and vice versa. We present results in the text for DMP-gene associations for *M. molossus* because it was the only short-lived species with a genome, but we summarize the DMP-gene associations for the other three species in Supplementary Fig. 5. Because we anticipated the mechanisms responsible for causing increases in methylation over time likely differs from those causing decreases, we conducted separate enrichment tests for genes with hypermethylated and hypomethylated sites associated with age and longevity using Panther v.16<sup>70</sup> in relation to biological process, molecular function, and protein class. We carried out enrichment tests using genes with DMPs in promoter regions because promoter regions showed enrichment for hypermethylated sites. To minimize redundancy due to the hierarchical organization of gene ontologies (GO), we present no more than three significant

(after FDR correction) GO terms from each parent-child group. All significant GO terms can be found in the Source Data files. We also used the significant age and longevity gene promoter lists to predict possible transcription factor regulators using BART, Binding Analysis for Regulation of Transcription<sup>47</sup>, which correlates the cis-regulatory profile derived from a gene set to the genomic binding profiles of 918 transcription regulators using over 7000 human ChIP-seq datasets. We report the Irwin-Hall P value, which indicates significance of the rank integrated over three test statistics<sup>47</sup>.

In addition, we carried out additional analyses to assess gene function using three relevant gene lists. The first utilized a list of 394 genes associated with changes in methylation over the lifespan of dogs<sup>17</sup>. This study assayed over 50,000 CpG sites for 104 known-aged labrador dogs, and included methylation data from mice and humans, to identify 198 hypermethylated and 196 hypomethylated sites, with most of the hypermethylated sites near genes associated with anatomical development. By comparing gene lists, we identified the number of positive (and negative) methylated genes in the dog list that occur in the genome of each bat, and then used the number of genes in the bat, as well as the number of age-related genes in the bat and the number that overlap to calculate the probability associated with overlap in each methylation direction. We used the R program phyper to conduct a Fisher's Exact Test (FET) using the hypergeometric distribution.

The second test utilized a list of 576 genes that have been documented to mutate frequently in over 10,864 human tumor cases. We downloaded v1.25.1 from the Genome Data Center of the National Cancer Institute (<https://portal.gdc.cancer.gov>). As with the dog age genes above, we calculated the probability of overlap between the cancer genes found in

the genomes of each of four bat species and both the bat age and longevity gene lists using a FET.

The third test involved comparing a list of 4,723 innate immunity genes downloaded from <https://www.innatedb.com> (Aug 14, 2020). As with the cancer gene list, we calculated the probability of overlap between the immunity genes found in the genome of the four bat genomes and both the bat age and longevity gene lists using a FET.

## Acknowledgements

This work was supported by the University of Maryland, College of Computer, Mathematical and Natural Sciences, a Paul G. Allen Frontiers Group grant to SH, an Irish Research Council Consolidator Laureate Award to ECT, and a UKRI Future Leaders Fellowship (MR/T021985/1) to SCV. SCV and PD were supported by a Max Planck Research Group awarded to SCV by the Max Planck Gesellschaft, and SCV and EZL were supported by a Human Frontiers Science Program Grant (RGP0058/2016) awarded to SCV.

We thank the Neurogenomics Core at UCLA for laboratory assistance, A. Lollar for providing *Tadarida* samples, M. Brooks for sharing a new maximum recorded lifespan for *Pteropus giganteus*, K. Bennett for graphical assistance, and to the Banbury Center, Cold Spring Harbor Labs for hosting the workshop that inspired this collaboration.

## Author contributions

G.S.W., D.M.A. and S.H. conceived and designed the study. D.M.A., B.D.A., H.C.B., G.G.C., L.N.C., D.K.N.D., P.D., N.J.F., A.V.G., L.G., E.H., G.J., M.K., E.Z.L., F.M., R.A.M., M.N., B.P., M.L.P., R.D.R., E.C.T., S.C.V., G.S.W., and D.Z. provided or prepared

samples. D.M.A., C.E.B, A.H., A.T.L., S.H., C.Z.L., J.A.R., G.S.W., J. Zhang and J. Zoller analyzed and interpreted data. G.S.W., D.M.A. and S.H. drafted the article. All authors provided comments to improve intellectual content and approve the final version.

### **Competing Interests**

SH is a founder of the non-profit Epigenetic Clock Development Foundation which plans to license several patents from his employer UC Regents. These patents list SH as inventor. The other authors declare no conflicts of interest.

### **Data availability**

The design of the Illumina microarray (HorvathMammalMethylChip40) used to generate the DNA methylation data is available from the Gene Expression Omnibus (GEO) at NCBI as platform GPL28271. Gene annotations for the microarray for ten bat genomes are available from the Digital Repository at the University of Maryland (DRUM) at <http://hdl.handle.net/1903/26373>. Normalized methylation values for each sample, along with sample metadata, are available from NCBI GEO. The coefficients from the penalized regressions used to estimate bat age are available at <https://doi.org/10.6084/m9.figshare.c.5257271>.

### **Code availability**

R code for implementing the analyses described in this paper is available at <https://doi.org/10.6084/m9.figshare.c.5257271>.

**Table 1.** Summary<sup>1</sup> of samples used for DNAm profiling.

<b><i>Genus species (Family)</i></b>	<b>Source</b>	<b>#F</b>	<b>#M</b>	<b>Exact N</b>	<b>Yg</b>	<b>Old</b>	<b>Max age</b>
<i>Antrozous pallidus (V)</i>	F	21	2	1	0.2	7	14.8
<i>Artibeus jamaicensis (Ph)</i>	C	3	0	2	11	13	19.2
<i>Carollia perspicillata (Ph)</i>	C	17	15	32	0.2	10.5	17.0
<i>Cynopterus brachyotis (Pt)</i>	C	6	4	10	6.7	12.9	13.0
<i>Desmodus rotundus (Ph)</i>	C	27	17	41	0.3	17.3	29.9
<i>Eidolon helvum (Pt)</i>	C	17	7	24	3.4	16.5	21.8
<i>Eptesicus fuscus (V)</i>	C	18	41	59	0.3	18.3	23.0
<i>Leptonycteris yerbabuenae (Ph)</i>	F	5	6	7	0.2	5	10.1
<i>Molossus molossus (M)</i>	F	9	5	6	0.3	5.9	5.9
<i>Myotis lucifugus (V)</i>	F	11	0	1	0.1	5	34.0
<i>Myotis myotis (V)</i>	F	36	2	33	1	9	37.1
<i>Myotis vivesi (V)</i>	F	11	6	4	0.1	2	10.0
<i>Nyctalus noctula</i>	F	3	0	2	0.9	2	12.0
<i>Phyllostomus discolor (Ph)</i>	C	31	19	42	0.1	17.7	18.0
<i>Phyllostomus hastatus (Ph)</i>	F	61	10	52	0.1	16.5	22.0
<i>Pteropus giganteus (Pt)</i>	C	0	4	4	10.9	14.2	44.0
<i>Pteropus hypomelanus (Pt)</i>	C	28	12	40	0.4	19.3	26.5
<i>Pteropus poliocephalus (Pt)</i>	C	10	6	16	6.1	16.7	23.6
<i>Pteropus pumilus (Pt)</i>	C	24	22	45	0.8	17.3	17.3
<i>Pteropus rodricensis (Pt)</i>	C	12	7	19	4	20.9	28.0
<i>Pteropus vampyrus (Pt)</i>	C	27	24	51	0.6	22.4	24.0
<i>Rhinolophus ferrumequinum (R)</i>	F	40	0	39	0.1	21.1	30.5
<i>Rhynchonycteris naso (E)</i>	F	6	16	15	0.1	6	8.5
<i>Rousettus aegyptiacus (Pt)</i>	C	8	8	3	5	14	22.9
<i>Saccopteryx bilineata (E)</i>	F	20	9	24	0.2	8.3	11.0
<i>Tadarida brasiliensis (M)</i>	C	9	10	15	0.2	6.2	12.0

<sup>1</sup>Family: E= Emballonuridae, M = Molossidae, Ph = Phyllostomidae, Pt = Pteropodidae, R = Rhinolophidae, V = Vespertilionidae; Source: F=field, C=captivity; #F, #M: number of samples for each sex; Exact N: number of individuals with exact age estimates; Yg, Old: youngest (Yg) and oldest (Old) individual sampled in years; Max age: maximum recorded age in years



## Figure Legends

**Fig. 1. Epigenetic clocks accurately predict chronological age of bats.** a) Leave-one-out (LOO) cross-validation based on penalized regression gave a correlation of 0.95 with a median absolute error (MAE) of 0.74 years between observed and predicted (DNAmAge) age (after square-root transform) for 26 bat species. To ensure an unbiased cross validation analysis, we allowed the number of CpGs to change with the respective training data. b) LOO cross-validation based on penalized regression of 51 *Pteropus vampyrus* samples gave a correlation of 0.99 with MAE of 0.72 years between observed and predicted age. c) LOO cross-validation based on penalized regression of 40 *Rhinolophus ferrumequinum* samples gave a correlation of 0.96 with MAE of 1.11 years between observed and predicted age. d) Cross-validation analysis in which the DNAm data for one species was left out (LOSO) and ages are predicted for that species using a clock estimated with the remaining data. The resulting correlation between observed and predicted age is 0.84 (MAE = 1.41 years). Additional epigenetic clocks for individual species and genera are in Supplementary Fig. 1 and 2.

**Fig. 2. Species longevity is predicted by mean rate of DNAm change.** a) After controlling for phylogeny using phylogenetic generalized least squares regression, mean DNAm rate at 1165 hypermethylating age DMPs correlate with longevity ( $r = -0.704$ ,  $t = -4.95$ ,  $P = 6.79e-5$ ), b) as does mean DNAm rate at 835 hypomethylating age DMPs ( $r = -0.682$ ,  $t = -4.27$ ,  $P = 3.42e-4$ ). Species longevity is represented by the longevity quotient (LQ), which is the ratio of the observed species maximum lifespan to the maximum lifespan predicted for a nonflying placental mammal of the same body mass<sup>29</sup>. For example, the maximum longevity of *Myotis*

*lucifugus* (10) is over six times longer than expected, while the maximum longevity of *Molossus molossus* (9) is equal to an average placental mammal of the same body size. The five species used for identifying longevity DMPs by difference in methylation rate are indicated by red triangles (long-lived) and blue triangles (short-lived). Only species with more than 10 samples are included.

**Fig. 3. Differentially methylated positions (DMPs) for age and longevity are widely distributed and partially overlap.** a) The top 2000 age-associated DMPs with positive (Pos) or negative (Neg) effects on DNAm are found on all *Rhinolophus ferrumequinum* chromosomes, although hypermethylated DMPs are underrepresented on chromosome 1 - syntenic with the human X chromosome. b) Longevity DMPs are also distributed across all *R. ferrumequinum* chromosomes. Darkened symbols indicate significance (BY 5% FDR). c) Effect of DNAm change on age plotted against effect of DNAm change on longevity (see Methods) illustrates association between age and longevity effects. Significant sites are colored blue for age, red for longevity, and purple for both age and longevity. Symbols for the orthologous gene with the nearest transcription start site (TSS) to the DMP are indicated for a sample of extreme age and longevity DMPs. Bottom panels indicate DMPs that map to different genes in the short-lived species, *M. molossus*, and the long-lived species, *R. ferrumequinum*, with the *M. molossus* gene indicated after /. Note that most extreme age and longevity DMPs in promoter regions (i.e. -10,000 to +1,000 bp from the tss) are in the upper right panel, i.e. nearest the same gene in both species. d) Age DMPs overlap 17% with hypermethylating (+) and hypomethylating (-) longevity DMPs in *M. molossus*. Long-lived bat species show similar patterns (Supplementary Fig. 5a). e) Number of unique genes nearest

age and longevity DMPs for *M. molossus*. Sign on numbers in overlap region indicate methylation direction for age then longevity. Long-lived bat species show similar patterns (Supplementary Fig. 5b).

**Fig. 4. Age and longevity DMPs are enriched in promoter regions of genes associated with immunity and cancer.** a) CpG annotation for the short-lived bat, *M. molossus*, in comparison to genome regions where probes map to the human genome (HG19) shows that only 49% of probes that map to a promoter region in the bat also map to a promoter region in human (see also Supplementary Fig. 4). b) In contrast, CpG annotation comparison between two phylogenetically distant bat species, *M. molossus* and *R. ferrumequinum*, indicates greater probe conservation with respect to gene proximity (see also Supplementary Fig. 4). c) Age DMPs are highly enriched near promoter regions with over 95% exhibiting hypermethylation in *M. molossus* and other bats (Supplementary Fig. 5). d) Longevity DMPs are also enriched in promoter regions with over 80% exhibiting hypermethylation in *M. molossus* and other bats (Supplementary Fig. 5). e) Enriched biological processes for unique *M. molossus* genes from promoter regions are only significant for hypermethylating age and longevity DMPs. Only three significant GO terms from each parent-child group are shown to minimize redundancy. f) Enrichment analysis of protein class for unique *M. molossus* genes from promoter regions reveals significant enrichment of helix-turn-helix transcription factors (TF) only for hypermethylated DMPs associated with age and longevity. Cell color indicates significance (negative log P for GO terms with  $\text{adjP} < 10\text{e-}4$ ) of enrichment in e) and f). g) Overlap between genes associated with longevity, innate immunity or frequently mutated in

human tumors identified in *M. molossus*. Enrichment analyses using genome annotations from other bat species produce similar results (Supplementary Fig. 6).

**Fig. 5. Functional overlap analysis of DMPs reveals role for key transcriptional regulators.** Histone marks for cell lines derived from skin, muscle or blood for DMPs mapped in *Desmodus rotundus*, a long lifespan species, for (a) age and (b) longevity with bold symbols indicating significance (BY 5% FDR) and +/- indicating positive/negative rates of DNAm change. Predicted chromatin states for cell lines derived from skin, muscle or blood for DMPs for (c) age and (d) longevity. e) Transcription factor clusters enriched for hypermethylated (+) and hypomethylated (-) age or longevity DMPs with cell color indicating significance (negative log P,  $\text{adjP} < 10\text{e-}4$ ) of overlap with predicted transcription factor binding sites in probe sequences using a hypergeometric test. f) Top-ranked transcription factors associated with change in expression of genes containing age or longevity DMPs in promoter regions in *M. molossus*, with integrative rank significance (see Methods) indicated as negative log P. Genes frequently mutated in human tumors are indicated by c, and those involved in innate immunity by i. Only genes with hypermethylated sites in promoter regions showed evidence of enrichment. Analyses using genome annotations from other bat species produce similar results (Supplementary Fig. 6).

## References

1. Razin A, Riggs AD. DNA methylation and gene function. *Science* 210, 604-610 (1980).
2. Chen Y, Breeze CE, Zhen S, Beck S, Teschendorff AE. Tissue-independent and tissue-specific patterns of DNA methylation alteration in cancer. *Epigenetics Chromatin* 9, 10 (2016).
3. Shemer R, Birger Y, Dean WL, Reik W, Riggs AD, Razin A. Dynamic methylation adjustment and counting as part of imprinting mechanisms. *Proc Natl Acad Sci U S A* 93, 6371-6376 (1996).
4. Gartler SM, Riggs AD. Mammalian X-chromosome inactivation. *Annu Rev Genet* 17, 155-190 (1983).
5. Choi J, Lyons DB, Kim MY, Moore JD, Zilberman D. DNA methylation and histone H1 jointly repress transposable elements and aberrant intragenic transcripts. *Mol Cell* 77, 310-323 e317 (2020).
6. Klutstein M, Nejman D, Greenfield R, Cedar H. DNA methylation in cancer and aging. *Cancer Res* 76, 3446-3450 (2016).
7. Unnikrishnan A, Hadad N, Masser DR, Jackson J, Freeman WM, Richardson A. Revisiting the genomic hypomethylation hypothesis of aging. *Ann N Y Acad Sci* 1418, 69-79 (2018).
8. Day K, *et al.* Differential DNA methylation with age displays both common and dynamic features across human tissues that are influenced by CpG landscape. *Genome Biol* 14, R102 (2013).
9. Rakyan VK, *et al.* Human aging-associated DNA hypermethylation occurs preferentially at bivalent chromatin domains. *Genome Res* 20, 434-439 (2010).
10. Teschendorff AE, *et al.* Age-dependent DNA methylation of genes that are suppressed in stem cells is a hallmark of cancer. *Genome Res* 20, 440-446 (2010).
11. Hannum G, *et al.* Genome-wide methylation profiles reveal quantitative views of human aging rates. *Mol Cell* 49, 359-367 (2013).
12. Horvath S. DNA methylation age of human tissues and cell types. *Genome Biol* 14, R115 (2013).
13. Stubbs TM, *et al.* Multi-tissue DNA methylation age predictor in mouse. *Genome Biol* 18, 68 (2017).

14. Thompson MJ, vonHoldt B, Horvath S, Pellegrini M. An epigenetic aging clock for dogs and wolves. *Aging* 9, 1055-1068 (2017).
15. Polanowski AM, Robbins J, Chandler D, Jarman SN. Epigenetic estimation of age in humpback whales. *Mol Ecol Res* 14, 976-987 (2014).
16. Wright PGR, *et al.* Application of a novel molecular method to age free-living wild Bechstein's bats. *Mol Ecol Res* 18, 1374-1380 (2018).
17. Wang T, *et al.* Quantitative translation of dog-to-human aging by conserved remodeling of the DNA methylome. *Cell systems* 11, 176-185 (2020).
18. Chen BH, *et al.* DNA methylation-based measures of biological age: meta-analysis predicting time to death. *Aging* 8, 1844-1865 (2016).
19. Marioni RE, *et al.* DNA methylation age of blood predicts all-cause mortality in later life. *Genome Biol* 16, 25 (2015).
20. Horvath S, Raj K. DNA methylation-based biomarkers and the epigenetic clock theory of ageing. *Nat Rev Genet* 19, 371-384 (2018).
21. Cole JJ, *et al.* Diverse interventions that extend mouse lifespan suppress shared age-associated epigenetic changes at critical gene regulatory regions. *Genome Biol* 18, 58 (2017).
22. Maegawa S, *et al.* Caloric restriction delays age-related methylation drift. *Nat Comm* 8, 539 (2017).
23. Lowe R, *et al.* Ageing-associated DNA methylation dynamics are a molecular readout of lifespan variation among mammalian species. *Genome Biol* 19, 22 (2018).
24. Sen P, Shah PP, Nativio R, Berger SL. Epigenetic mechanisms of longevity and aging. *Cell* 166, 822-839 (2016).
25. Marttila S, *et al.* Ageing-associated changes in the human DNA methylome: genomic locations and effects on gene expression. *BMC genomics* 16, 179-179 (2015).
26. Kane AE, Sinclair DA. Epigenetic changes during aging and their reprogramming potential. *Crit Rev Biochem Mol Biol* 54, 61-83 (2019).
27. McLain AT, Faulk C. The evolution of CpG density and lifespan in conserved primate and mammalian promoters. *Aging* 10, 561-572 (2018).
28. Mayne B, Berry O, Davies C, Farley J, Jarman S. A genomic predictor of lifespan in vertebrates. *Sci Rep* 9, 17866 (2019).

29. Wilkinson GS, Adams DM. Recurrent evolution of extreme longevity in bats. *Biol Lett* 15, 20180860 (2019).
30. Ahn M, *et al.* Dampened NLRP3-mediated inflammation in bats and implications for a special viral reservoir host. *Nat Microbiol* 4, 789-799 (2019).
31. Gorbunova V, Seluanov A, Kennedy BK. The world goes bats: living longer and tolerating viruses. *Cell Metab* 32, 31-43 (2020).
32. Amador LI, Arevalo RLM, Almeida FC, Catalano SA, Giannini NP. Bat systematics in the light of unconstrained analyses of a comprehensive molecular supermatrix. *J Mamm Evol* 25, 37-70 (2018).
33. Dixon JR, *et al.* Topological domains in mammalian genomes identified by analysis of chromatin interactions. *Nature* 485, 376–380 (2012).
34. Breeze CE, *et al.* eFORGE v2.0: updated analysis of cell type-specific signal in epigenomic data. *Bioinformatics* 35, 4767-4769 (2019).
35. Arthur RK, An N, Khan S, McNerney ME. The haploinsufficient tumor suppressor, CUX1, acts as an analog transcriptional regulator that controls target genes through distal enhancers that loop to target promoters. *Nucleic Acids Res* 45, 6350-6361 (2017).
36. Wilsker D, Patsialou A, Dallas PB, Moran E. ARID proteins: a diverse family of DNA binding proteins implicated in the control of cell growth, differentiation, and development. *Cell Growth Differ* 13, 95-106 (2002).
37. Engelmann D, Putzer BM. The dark side of E2F1: in transit beyond apoptosis. *Cancer Res* 72, 571-575 (2012).
38. Kim W, *et al.* ZFP161 regulates replication fork stability and maintenance of genomic stability by recruiting the ATR/ATRIP complex. *Nat Comm* 10, 5304 (2019).
39. Zhou P, *et al.* IRF7 in the Australian black flying fox, *Pteropus alecto*: evidence for a unique expression pattern and functional conservation. *PloS one* 9, e103875 (2014).
40. Li L, *et al.* TFAP2C- and p63-dependent networks sequentially rearrange chromatin landscapes to drive human epidermal lineage commitment. *Cell Stem Cell* 24, 271-284 e278 (2019).
41. Orso F, *et al.* AP-2alpha and AP-2gamma regulate tumor progression via specific genetic programs. *Faseb J* 22, 2702-2714 (2008).
42. Poulin H, Labelle Y. The PLAGL1 gene is down-regulated in human extraskeletal myxoid chondrosarcoma tumors. *Cancer Lett* 227, 185-191 (2005).

43. De Keersmaecker K, *et al.* Exome sequencing identifies mutation in CNOT3 and ribosomal genes RPL5 and RPL10 in T-cell acute lymphoblastic leukemia. *Nat Genet* 45, 186-190 (2013).
44. Shirai YT, *et al.* CNOT3 targets negative cell cycle regulators in non-small cell lung cancer development. *Oncogene* 38, 2580-2594 (2019).
45. Kumar S. P53 induction accompanying G2/M arrest upon knockdown of tumor suppressor HIC1 in U87MG glioma cells. *Mol Cell Biochem* 395, 281-290 (2014).
46. Lambert SA, *et al.* The human transcription factors. *Cell* 172, 650-665 (2018).
47. Wang Z, Civelek M, Miller CL, Sheffield NC, Guertin MJ, Zang C. BART: a transcription factor prediction tool with query gene sets or epigenomic profiles. *Bioinformatics* 34, 2867-2869 (2018).
48. Lu T, *et al.* REST and stress resistance in ageing and Alzheimer's disease. *Nature* 507, 448-454 (2014).
49. Petkovich DA, Podolskiy DI, Lobanov AV, Lee SG, Miller RA, Gladyshev VN. Using DNA methylation profiling to evaluate biological age and longevity interventions. *Cell Metab* 25, 954-960 e956 (2017).
50. Christensen BC, *et al.* Aging and environmental exposures alter tissue-specific DNA methylation dependent upon CpG island context. *PLoS Genet* 5, e1000602 (2009).
51. Faure PA, Re DE, Clare EL. Wound healing in the flight membranes of big brown bats. *J Mammal* 90, 1148-1156 (2009).
52. Cheney JA, Allen JJ, Swartz SM. Diversity in the organization of elastin bundles and intramembranous muscles in bat wings. *J Anat* 230, 510-523 (2017).
53. Olds JE, *et al.* Retrospective evaluation of cases of neoplasia in a captive population of Egyptian fruit bats (*Rousettus aegyptiacus*). *J Zoo Wildl Med* 46, 325-332 (2015).
54. Seim I, *et al.* Genome analysis reveals insights into physiology and longevity of the Brandt's bat *Myotis brandtii*. *Nat Comm* 4, 2212 (2013).
55. Huang Z, Jebb D, Teeling EC. Blood miRNomes and transcriptomes reveal novel longevity mechanisms in the long-lived bat, *Myotis myotis*. *BMC genomics* 17, 906 (2016).
56. Banerjee A, Baker ML, Kulcsar K, Misra V, Plowright R, Mossman K. Novel insights into immune systems of bats. *Front Immunol* 11, 26 (2020).



57. Arneson A, *et al.* A mammalian methylation array for profiling methylation levels at conserved sequences. *bioRxiv*, (2021).
58. Zhou W, Triche TJ, Jr., Laird PW, Shen H. SeSAME: reducing artifactual detection of DNA methylation by Infinium BeadChips in genomic deletions. *Nucleic Acids Res* 46, e123 (2018).
59. Gaidatzis D, Lerch A, Hahne F, Stadler MB. QuasR: quantification and annotation of short reads in R. *Bioinformatics* 31, 1130-1132 (2015).
60. Yu G, Wang LG, He QY. ChIPseeker: an R/Bioconductor package for ChIP peak annotation, comparison and visualization. *Bioinformatics* 31, 2382-2383 (2015).
61. Friedman J, Hastie T, Tibshirani R. Regularization paths for generalized linear models via coordinate descent. *J Stat Software* 33, 1-22 (2010).
62. Stouffer SA, Suchman EA, DeVinney LC, Star SA, Williams RMJ. *The American Soldier, Vol I: Adjustment during Army Life*. Princeton University Press (1949).
63. Jebb D, *et al.* Six reference-quality genomes reveal evolution of bat adaptations. *Nature* 583, 578-584 (2020).
64. Benjamini Y, Yekutieli D. The control of the false discovery rate in multiple testing under dependency. *Ann Stat* 29, 1165-1188 (2001).
65. Matys V, *et al.* TRANSFAC and its module TRANSCompel: transcriptional gene regulation in eukaryotes. *Nucleic Acids Res* 34, D108-110 (2006).
66. Hume MA, Barrera LA, Gisselbrecht SS, Bulyk ML. UniPROBE, update 2015: new tools and content for the online database of protein-binding microarray data on protein-DNA interactions. *Nucl Acids Res* 43, D117-122 (2015).
67. Yin Y, *et al.* Impact of cytosine methylation on DNA binding specificities of human transcription factors. *Science* 356, (2017).
68. Fornes O, *et al.* JASPAR 2020: update of the open-access database of transcription factor binding profiles. *Nucl Acids Res* 48, D87-D92 (2020).
69. Maurano MT, *et al.* Large-scale identification of sequence variants influencing human transcription factor occupancy in vivo. *Nat Genet* 47, 1393-1401 (2015).
70. Mi H, *et al.* Protocol Update for large-scale genome and gene function analysis with the PANTHER classification system (v.14.0). *Nature protocols* 14, 703-721 (2019).

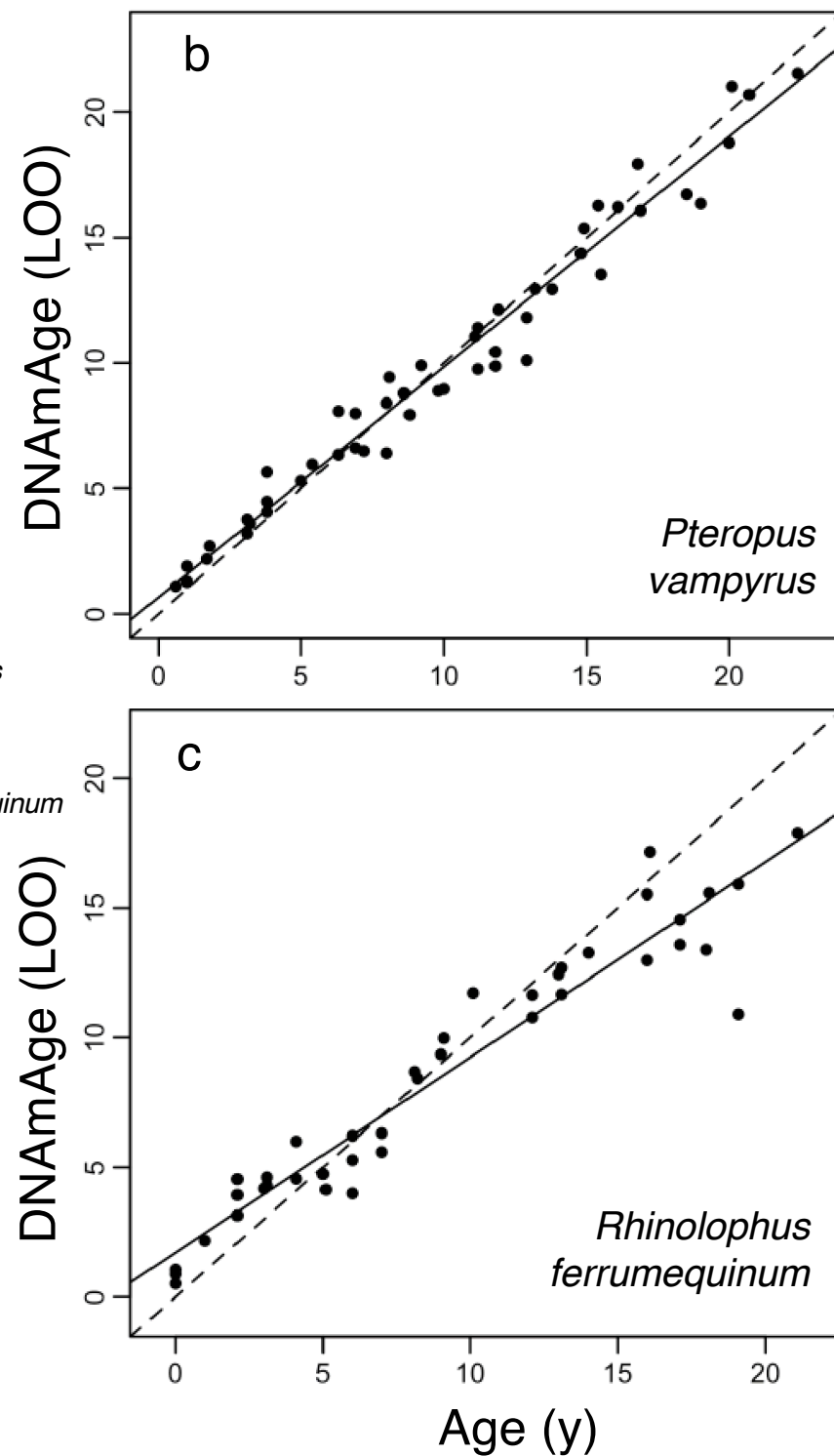
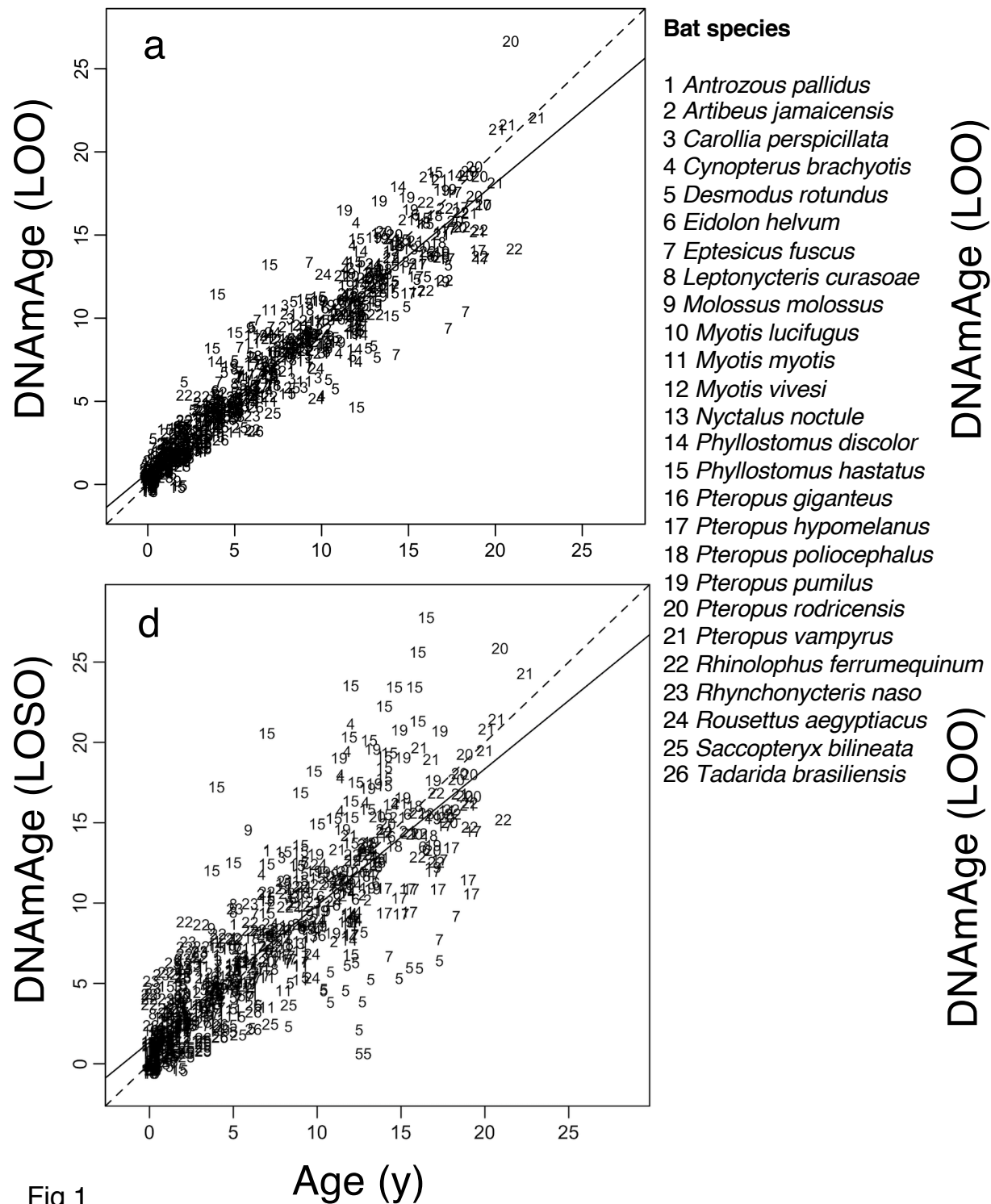


Fig 1

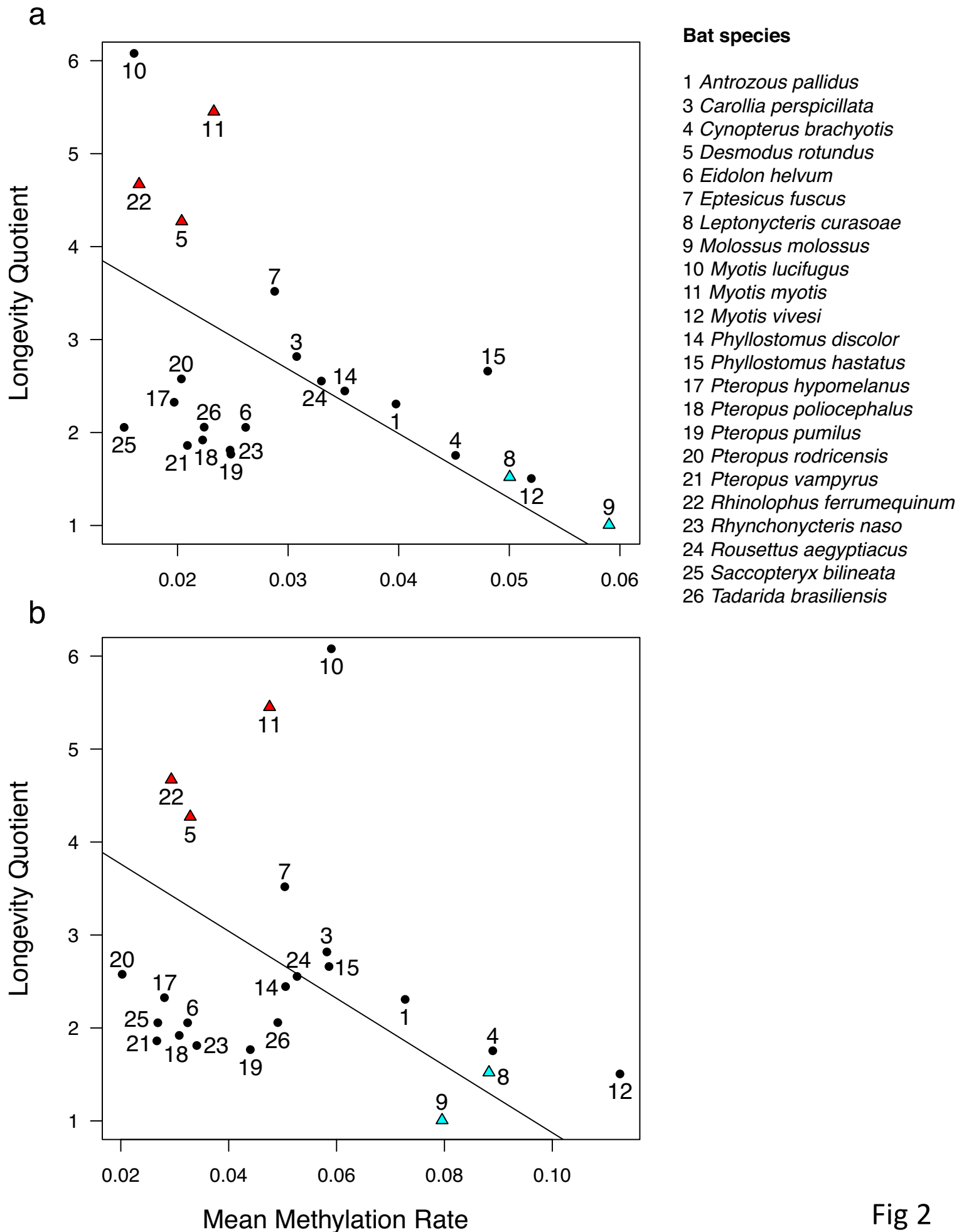
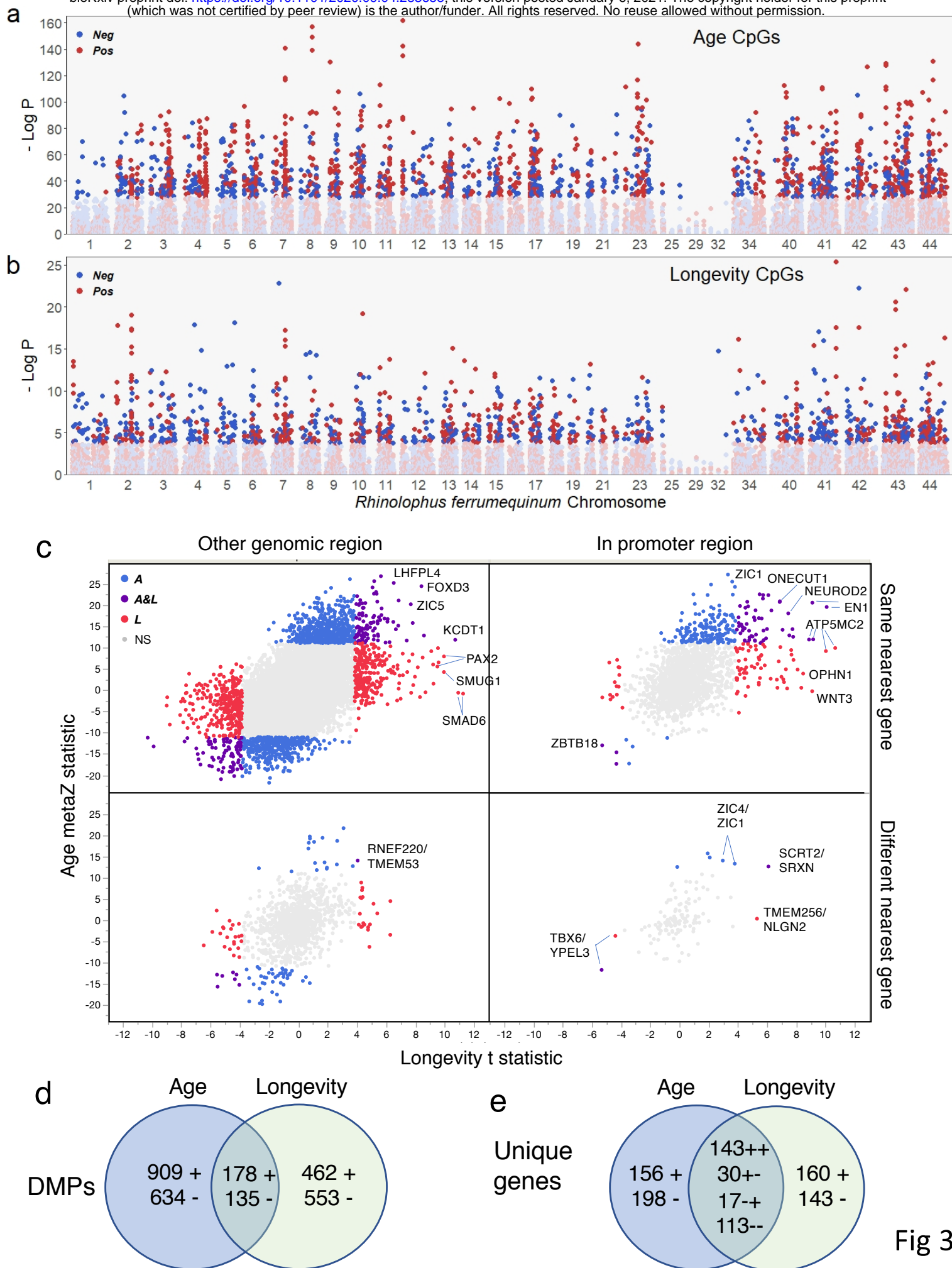


Fig 2



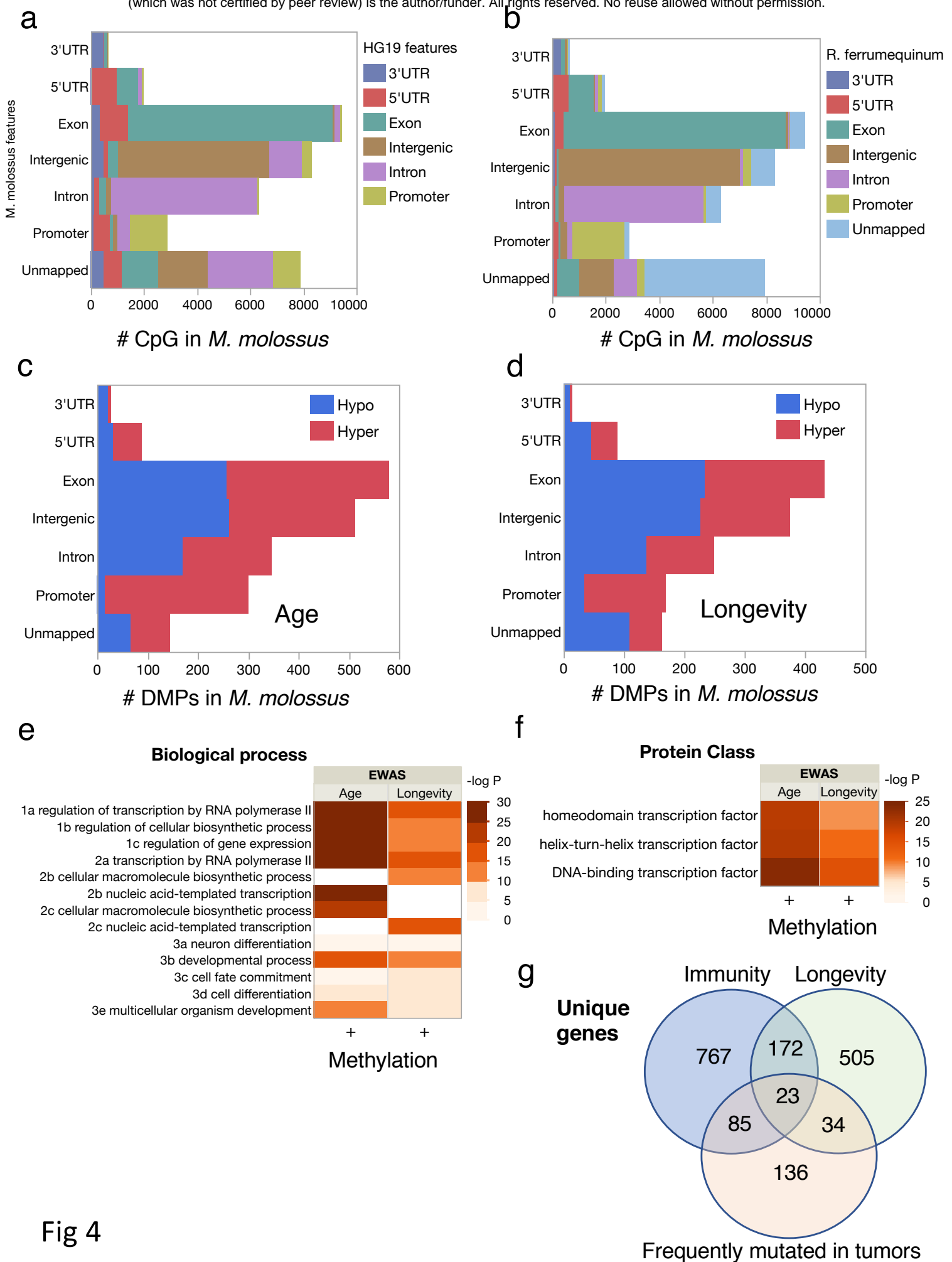


Fig 4

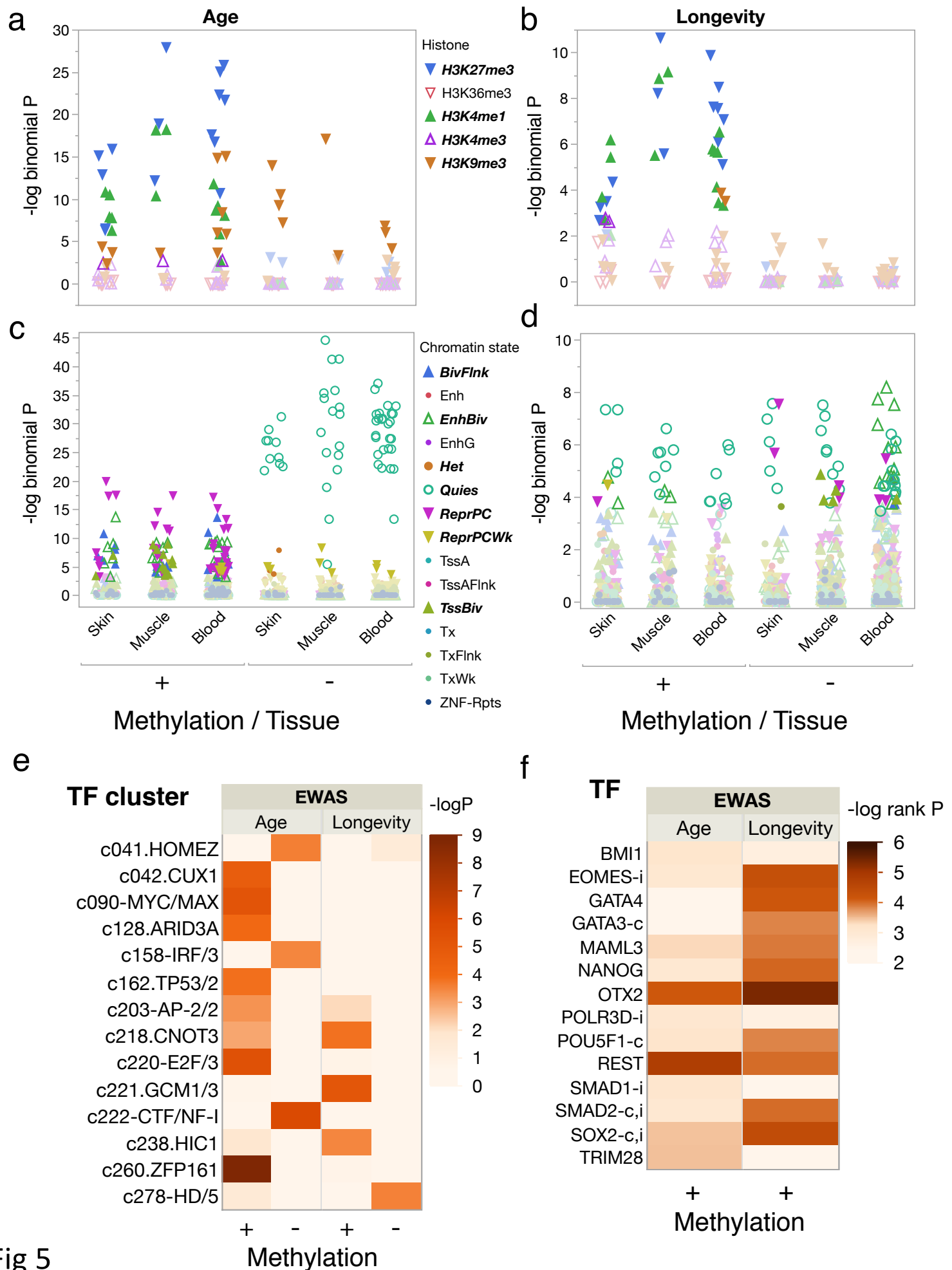


Fig 5